Nanoscale

Accepted Manuscript

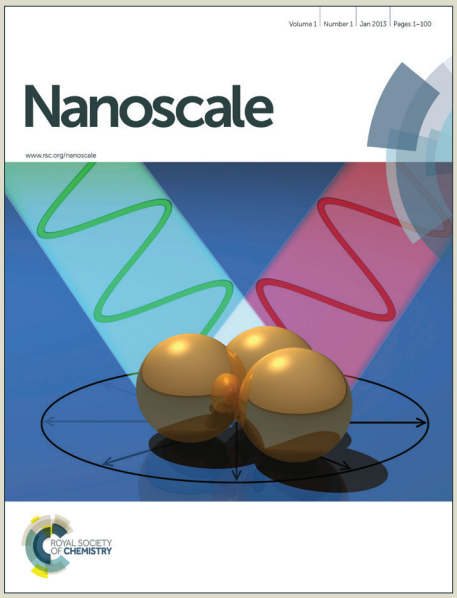

Multi-modular, tris(triphenylamine) zinc porphyrin – zinc phthalocyanine –fullerene conjugate as a broad-band capturing, charge stabilizing, photosynthetic 'antenna-reaction center' mimic†

Chandra B. KC, Gary N. Lim, and Francis D'Souza*

*Received *** ; Revised*** ; Accepted****
DOI:

Department of Chemistry, University of North Texas, 1155 Union Circle, #305070, Denton, TX 76203-5017, USA

E-mail: Francis.DSouza@unt.edu

†Electronic supplemental information (ESI) available: Energy level diagram showing multi-step energy transfer process in $(TPA)_3ZnP$-ZnPc; Job's plot for stoichiometry determination, voltammograms of control compounds, spectrum of chemically oxidized $(TPA)_4ZnP$, femtosecond transient spectra of control conjugates and ZnPc, Nanosecond transient spectra of $(TPA)_4ZnP$, and $(TPA)_4ZnP$:ImC_{60}; MALDI-TOF-mass, ^1H and ^{13}C NMR spectra of $(TPA)_3ZnP$-ZnPc. See DOI:

(Abstract) A broad-band capturing, charge stabilizing, photosynthetic antenna-reaction center model compound has been newly synthesized and characterized. The model compound is comprised of a zinc porphyrin covalently linked to three units of triphenylamine entities and a zinc phthalocyanine entity. The absorption and fluorescence spectra of zinc porphyrin complemented that of zinc phthalocyanine offering broad-band coverage. Stepwise energy transfer from singlet excited triphenylamine to zinc porphyrin, and singlet excited zinc porphyrin to zinc phthalocyanine ($k_{ENT} \sim 10^{11}$ s^{-1}) was established from spectroscopic and time-resolved transient absorption techniques. Next, an electron acceptor, fullerene was introduced via metal-ligand axial coordination to both zinc porphyrin and zinc phthalocyanine centers, and were characterized by spectroscopic and electrochemical techniques. An association constant of 4.9 x 10^4 M^{-1} for phenylimidazole functionalized fullerene binding to zinc porphyrin, and 5.1 x 10^4 M^{-1} for it binding to zinc phthalocyanine were obtained. Energy level diagram for the occurrence of different photochemical events within the multi-modular donor-acceptor conjugate was established from spectral and electrochemical data. Unlike the previous zinc porphyrin-zinc phthalocyanine-fullerene conjugates, the newly assembled donor-acceptor conjugate has been shown to undergo the much anticipated initial charge separation from singlet excited zinc porphyrin to the coordinated fullerene followed by a hole shift process to zinc phthalocyanine resulting into a long-lived charge separated state as revealed by femto- and nanosecond transient absorption spectroscopic techniques. The lifetime of the final charge separated state was about 100 ns.

Introduction

Multi-step energy transfer followed by sequential electron transfer leading to the formation of charge separated states of appreciable lifetimes in model photosynthetic systems is one of the highly sought out functional nanoscale materials[1-10] for building low-cost, light-to-electricity and light-to-fuel converting devices.[11-14] This goal has often been accomplished by a multi-modular approach wherein carefully selected antenna entity(ies) are linked to the electron donor entity of a donor-acceptor pair. The antenna entities with their complimentary absorption and emission to the primary electron donor and acceptor entities help in capturing light from the useful portion of the electromagnetic spectrum, that is, maximum utilization of solar energy. Both covalent and self-assembly approaches have been used in building such multi-modular systems. Interestingly, a combination of these two approaches is found to be highly useful as this approach provides better control for a systematic understanding of the different photochemical events originating in quite multifaceted, 'antenna-reaction center' model compounds.[6]

Among the different model compounds revealing sequential energy and electron transfer, multi-modular systems comprised of BODIPY-porphyrin-fullerene (BODIPY = BF_2-chelated dipyrromethene)[15-16] and porphyrin-phthalocyanine-fullerene[17-19] have been some of the successful ones. This is primarily due to the complimentary absorption and emission of the different entities covering different portions of the spectrum, synthetic versatility, well-established redox and photochemical properties, and ability of fullerene to produce long-lived charge separated states in donor-acceptor systems.[20-21] Wealth of information, otherwise difficult to gather, have been secured from these studies involving model compounds developed using these molecular building blocks and photosynthetic principles. However, to-date, a long-lived charge separated state in porphyrin-phthalocyanine-fullerene conjugates was not possible to establish due to competing energy and electron transfer processes.[17-19]

In the present study, this has been accomplished by building a novel multi-modular 'antenna-reaction center' model compound comprised of covalently linked zinc porphyrin-zinc phthalocyanine dyad. Occurrence of singlet-singlet energy transfer in porphyrin-phthalocyanine is well-known[17-19] and a similar effect is anticipated here also. However, in the current model compound, the porphyrin *meso*-positions have been substituted with three triphenylamine units. These triphenylamine entities fulfill the role of additional antenna that would capture light from the 300 nm range and funnel it to the porphyrin center. In addition, the *meso*-triphenylamine

substituted porphyrin is known to stabilize charge separated states in donor-acceptor dyads.[22] Finally, phenylimidazole functionalized fullerene[23] has been utilized as an electron acceptor via metal-ligand axial coordination of $(TPA)_3ZnP$-ZnPc to form $(TPA)_3ZnP$:ImC_{60}-ZnPc:ImC_{60} conjugate (see Scheme 1 for structures). Systematic studies have been performed using various physico-chemical and photochemical techniques to establish 'antenna-reaction center' events and charge stabilization in these wide-band capturing multi-modular systems.

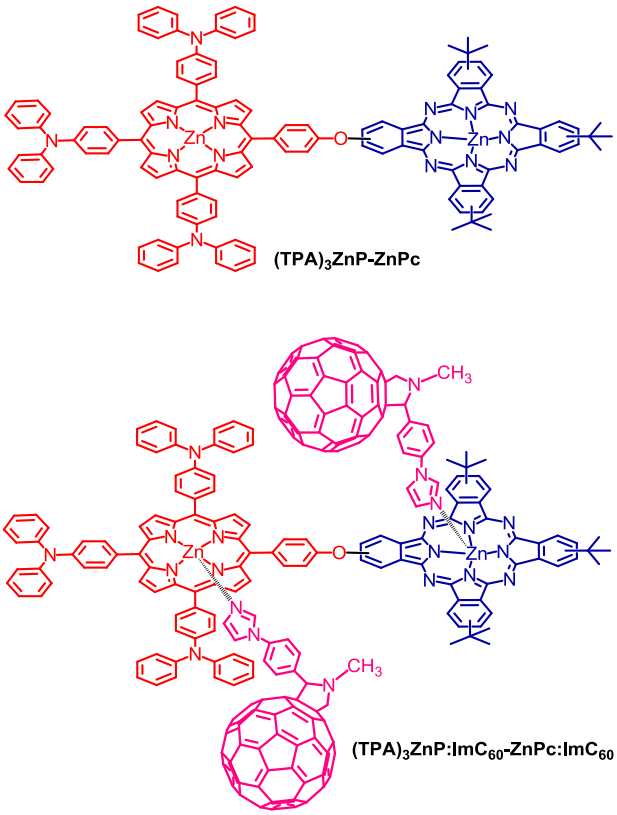

Scheme 1. Structures of the tris(triphenylamine) zinc porphyrin-zinc phthalocyanine, $(TPA)_3ZnP$–ZnPc and its fullerene complex, $(TPA)_3ZnP$:ImC_{60}-ZnPc:ImC_{60} developed as broad-band capturing, charge stabilizing, photosynthetic 'antenna-reaction center' mimic in the present study. The symbol ':' represents coordinate zinc-nitrogen bond.

Results and discussion

Synthesis of tri(triphenylamine) zinc porphyrin – zinc phthalocyanine, $(TPA)_3ZnP$–ZnPc

The synthesis of this molecule carried out according to Scheme 2 and the details are given in the experimental section. Briefly, 4-(4-formylphenoxy)phthalonitrile was obtained by the

reaction of 4-nitrophthalonitrile and 4-hydroxybenzaldehyde in DMF. Next, [5-(4-(4-phenoxy)phthalonitrile)-10,15,20- tris(4-triphenylamino) porphyrin] was synthesized by 4-(4-formylphenoxy)phthalonitrile (1 eq.), 4-(diphenylamino)benzaldehyde (3 eq.) and pyrrole (4 eq.) in propionic acid followed by chromatographic separation on silica gel column. Next, $(TPA)_3$ZnP-ZnPc was synthesized by reaction *t*-butyl phthalonitrile, porphyrin derivative from the previous step, and $ZnCl_2$ in dimethylaminoethanol followed by chromatographic purification. Purity of the newly synthesized compounds was ascertained by thin-layer chromatography and the structural integrity was established from ^{1}H and ^{13}C NMR, MALDI-TOF-Mass, spectral and electrochemical studies. The compounds were stored in dark prior doing spectral and transient spectral measurements.

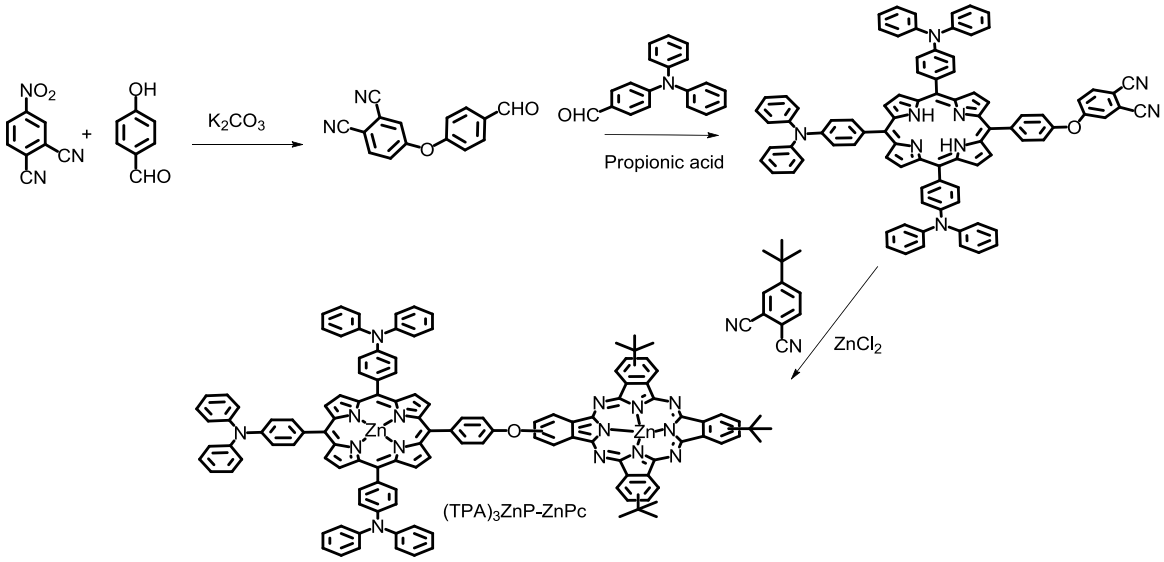

Scheme 2. Synthetic methodology adopted for $(TPA)_3$ZnP-ZnPc.

Absorption and fluorescence studies

Fig. 1a shows the absorption spectrum of $(TPA)_3$ZnP-ZnPc along with the control compounds in *o*-dichlorobenzene (DCB). Absorption bands of $(TPA)_3$ZnP-ZnPc were located at 315, 348, 435, 556, 613 and 680 nm. The zinc porphyrin Soret band of $(TPA)_3$ZnP-ZnPc located at 435 nm was red-shifted by 15 nm compared to tetraphenylporphyrinatozinc(II) (ZnTPP) and was broadened significantly due to the presence of triphenylamine (TPA) entities at the ring periphery.[22] Similarly, the TPA peak at 305 nm was blue-shifted by 55 nm compared to control,

4-(diphenylamino)benzaldehyde, TPA-CHO (360 nm). The zinc phthalocyanine intense visible band in $(TPA)_3$ZnP-ZnPc was located at 682 nm which is not significantly different from that of pristine ZnPc (=*t*-butyl zinc phthalocyanine). These results revealed weak intramolecular interactions, if any, between the entities of the $(TPA)_3$ZnP-ZnPc and a broad spectral coverage from 300 to 750 nm.

Fig. 1b and c show the fluorescence spectrum of $(TPA)_3$ZnP-ZnPc along with the control compounds in DCB at the excitation wavelength corresponding to TPA-CHO and ZnP, respectively. Emission of control compounds, TPA-CHO at 485 nm, ZnTPP at 600 and 648 nm, $(TPA)_4$ZnP at 620 and 660(sh) nm, and ZnPc at 695 nm, when excited at their respective absorption peak maxima were observed. As shown in Fig. 1b, the TPA fluorescence was quenched over 97% in $(TPA)_3$ZnP-ZnPc. Scanning the wavelength beyond 550 nm revealed a peak at 620 nm corresponding to ZnP in the case of $(TPA)_4$ZnP, and at 695 nm corresponding to ZnPc (see Fig. S12 in ESI for ZnPc emission spectrum) in the case of $(TPA)_3$ZnP-ZnPc suggesting occurrence of energy transfer from ^{1}TPA* to ZnP in the case of $(TPA)_4$ZnP, and a two-step process, viz., ^{1}TPA* to ZnP to yield ^{1}ZnPc* followed by a second energy transfer process between ^{1}ZnP* and ZnPc to yield ^{1}ZnP*. Occurrence of energy transfer from ^{1}ZnP* to ZnPc yielding ^{1}ZnPc* is demonstrated in Fig. 1c when $(TPA)_3$ZnP-ZnPc was excited at the ZnP peak maxima at 438 nm (similar effect was also observed by Soret band excitation). Under these conditions, $(TPA)_3$ZnP emission expected at 620 nm was fully quenched with the appearance of peaks corresponding to ZnPc. Further, excitation spectrum of $(TPA)_3$ZnP-ZnPc was recorded by holding the emission monochromator to 695 nm (corresponding to ZnPc emission) and scanning the excitation wavelength, as shown in Fig. 1d. The spectrum revealed peaks of not only ZnPc but also those of ZnP and TPA entities, confirming a two-step energy transfer process.[24] An estimation of energy transfer efficiency by taking the intensity ratio of ZnP/ZnPc bands (570 nm/630 nm) in the absorption and excitation spectra, revealed it to be about 94%, implying very efficient energy transfer.

Fig. S1 in electronic supplementary information (ESI) provides an energy level diagram revealing double excitation transfer in $(TPA)_3$ZnP-ZnPc. Selective excitation of $(TPA)_3$ZnP at the TPA absorption maxima (hν in Fig. S1) populates the ^{1}ZnP* via ENT-1 process. The close proximity governed intramolecular interactions between TPA entities and ZnP macrocycle facilitates such excitation process. The ^{1}ZnP* formed either via energy transfer from excited

TPA (ENT-1) or by direct excitation (hν'), undergoes singlet-singlet energy transfer to ZnPc (ENT-2) in competition with an intersystem crossing process to populate ^{3}ZnP* (ISC). Femtosecond transient spectral measurements were performed to probe kinetics of the ENT-2 process and these results will be discussed in the latter section.

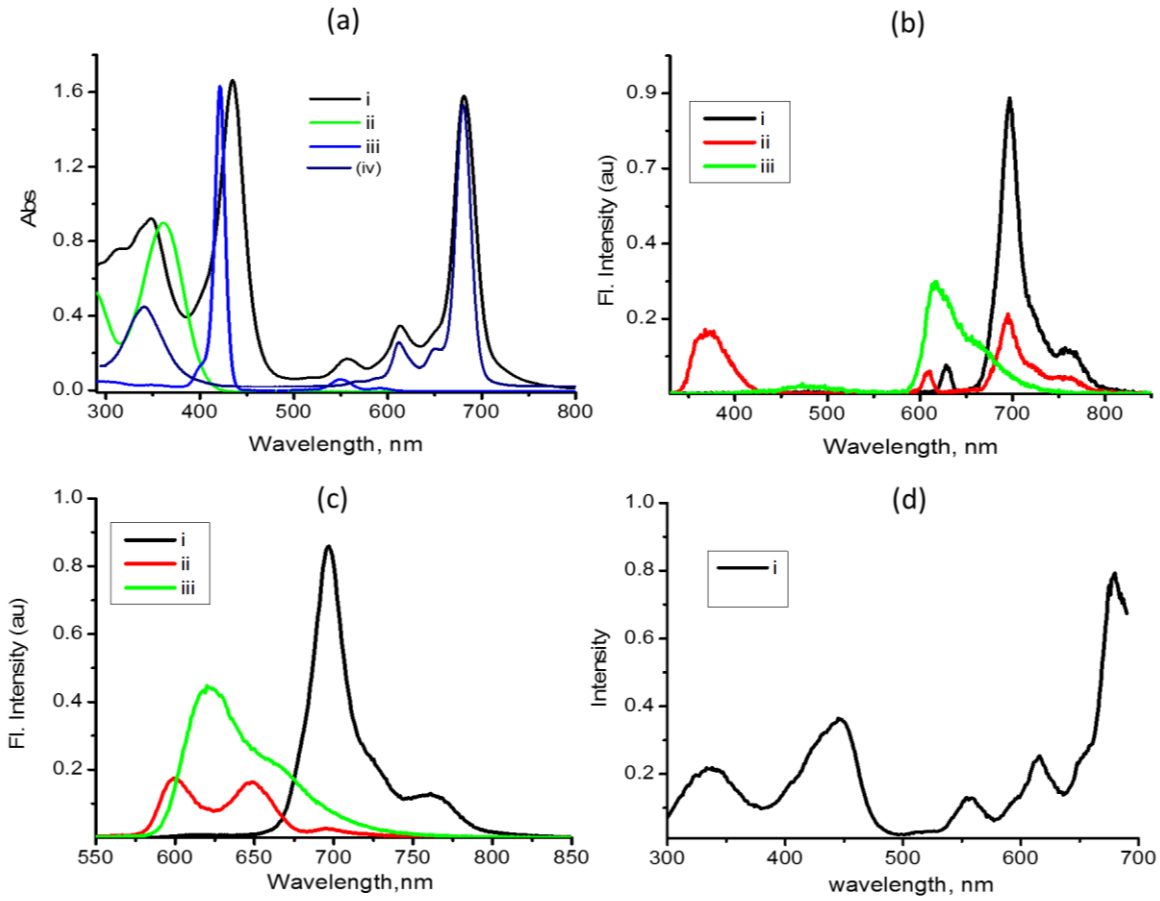

Fig. 1. (a) Normalized to the Soret band absorption spectrum of (i) $(TPA)_3$ZnP-ZnPc, (ii) TPA-CHO, (iii) ZnTPP, and (iv) ZnPc in DCB. (b) Fluorescence spectrum (λ_{ex} = 315 nm) of (i) $(TPA)_3$ZnP-ZnPc, (ii) a mixture of TPA-CHO (3 eq.)+ZnTPP (1 eq.)+ZnPc (1 eq.), and (iii) $(TPA)_4$ZnP in DCB. (c) Fluorescence spectrum (λ_{ex} = 432 nm) of (i) $(TPA)_3$ZnP-ZnPc, (ii) a mixture of TPA-CHO (3 eq.)+ZnTPP (1 eq.)+ZnPc (1 eq.), and (iii) $(TPA)_4$ZnP in DCB. (d) Excitation spectrum of $(TPA)_3$ZnP-ZnPc in DCB recorded by holding the emission monochromator to 696 nm corresponding to ZnPc emission.

Formation and characterization of $(TPA)_3$ZnP:ImC_{60}-ZnPc:C_{60}Im conjugate

The presence of coordinatively unsaturated zinc metal ions in $(TPA)_3$ZnP-ZnPc provided us an oppurtunity to build donor-acceptor conjugate by metal-ligand axial coordination

approach.[22] For this, we have utilized electron acceptor fullerene bearing a phenylimidazole ligating group, C_{60}Im. The presence of two Zn centers in $(TPA)_3$ZnP-ZnPc allows the coordination of two equivalents of C_{60}Im to yield $(TPA)_3$ZnP:ImC_{60}-ZnPc:ImC_{60} conjugate. Fig. 2 shows the spectral changes observed during increased addition of C_{60}Im to a solution of $(TPA)_3$ZnP-ZnPc in DCB. The porphyrin Soret band revealed characteristic spectral changes

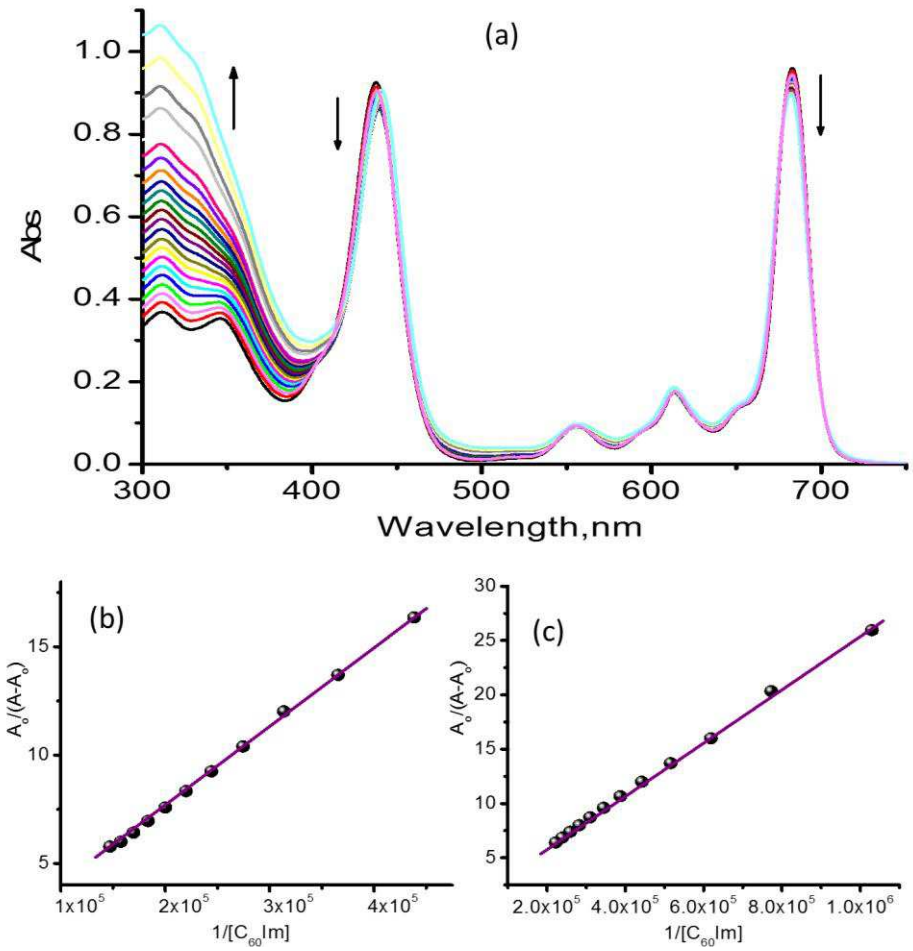

Fig. 2. (a) Absorption spectral changes observed for C_{60}Im (3.8 mM, 2.0 μL each addition) binding to $(TPA)_3$ZnP-ZnPc (3.5 μM) in DCB. Fig. b and c show Benesi-Hildebrand plots, at the monitoring wavelengths of 432 nm band for ZnP and 682 nm for ZnPc, to calculate the binding constants.

associated with zinc porphyrin binding to a nitrogenous ligand.[23a,b] That is, an initial decrease of the Soret band intensity followed by an increase with noticeable red-shift (~7 nm) upon further addition of C_{60}Im. The 682 nm band corresponding to ZnPc also revealed a decrease in intensity upon C_{60}Im binding.[23c] These spectral changes are consistent with C_{60}Im binding to

the zinc centers of both macrocycles.[23] The absorbance data was analyzed to evaluate the binding constants (Soret band for $(TPA)_3ZnP:ImC_{60}$ formation and 682 nm band for $ZnPc:C_{60}Im$ formation) by constructing Benesi-Hildebrand plots[25] as shown in Fig. 2b and 2c. Such plots yielded values of 4.9 x 10^4 M^{-1} for $(TPA)_3ZnP:ImC_{60}$ formation, and 5.1 x 10^4 M^{-1} for $ZnPc:C_{60}Im$ formation within the conjugate; not significantly different from one another. Further, Job's plots were constructed to evaluate the stoichiometry of the coordinated complex (see Fig. S2 in ESI). Analysis of porphyrin Soret and phthalocyanine visible bands with respect to added $C_{60}Im$ revealed 1:1 stoichiometry for the two metal centers, suggesting that $(TPA)_3ZnP$ and ZnPc act as s independent binding sites without any cooperative effects.

The fluorescence spectrum of $(TPA)_3ZnP$-ZnPc in the presence of $C_{60}Im$ at both ZnP excitation (555 nm) and ZnPc excitation (682 nm) wavelengths were recorded, as shown in Fig. 3. Quenching of fluorescence emission was observed at both the excitation wavelengths suggesting excited state events in $(TPA)_3ZnP:ImC_{60}$-$ZnPc:C_{60}Im$ either by ZnP or ZnPc excitation.

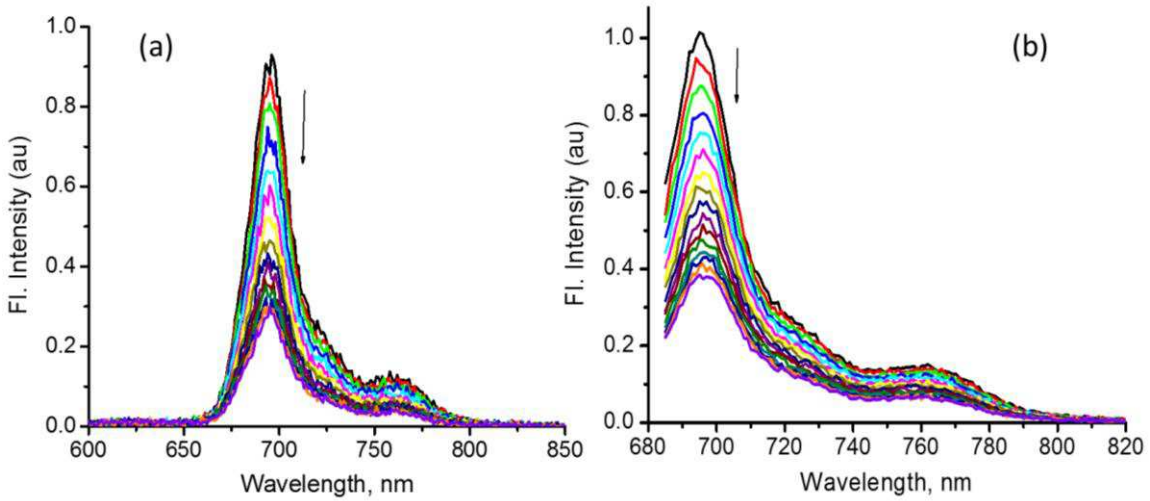

Fig. 3. Fluorescence spectrum of $(TPA)_3ZnP$-ZnPc upon increasing addition of $C_{60}Im$ (a) at the excitation wavelength of 555 nm corresponding to ZnP and (b) at the excitation wavelength of 682 nm corresponding to ZnPc in DCB.

Electrochemistry and energy level diagram

Electrochemical studies using differential pulse voltammetry (DPV) were performed to evaluate the redox potentials of $(TPA)_3ZnP:ImC_{60}$-$ZnPc:ImC_{60}$ conjugate, and also to evaluate

the energetics of the different photochemical processes. Both zinc porphyrin and zinc phthalocyanine are known to undergo two one-electron reductions leading to the formation of π-radical anion and dianion species, and two one-electron oxidations leading to the formation of π-radical cation and dication species, respectively.[26] Having additional electroactive groups on the macrocyclic periphery, such as the TPA entities in case of $(TPA)_3$ZnP-ZnPc would result in additional redox peaks.[27] Fig. 4 shows a DPVs of the $(TPA)_3$ZnP-ZnPc in the presence and absence of C_{60}Im in DCB, 0.1 M (n-$Bu_4N)ClO_4$. For $(TPA)_3$ZnP-ZnPc, three oxidation processes located at -0.06, 0.11, and 0.80 V vs. Fc/Fc^+ were observed during anodic excursion while three reductions at -1.66, -1.84 and -1.99 V vs. Fc/Fc^+ were observed during cathodic excursion of the potential within the potential window of the solvent. By comparing the voltammograms of pristine $(TPA)_4$ZnP and ZnPc (see Fig. S3 in ESI for voltammograms), the first two oxidation process were ascribed to the formation of $ZnPc^{\bullet+}$ and $ZnPc^{2+}$ species, respectively, while the third oxidation was attributed to the formation of $ZnP^{\bullet+}$. Additional multi-electron oxidation at higher anodic potential was also observed due to the presence of TPA entities[27] (data not shown). The first two reductions were attributed to the formation of $ZnP^{\bullet-}$ and $ZnPc^{\bullet-}$, respectively. Increasing addition of C_{60}Im to form $(TPA)_3$ZnP:ImC_{60}-ZnPc:C_{60}Im conjugate revealed significant changes. That is, the currents of the first oxidation process of ZnPc and ZnP revealed

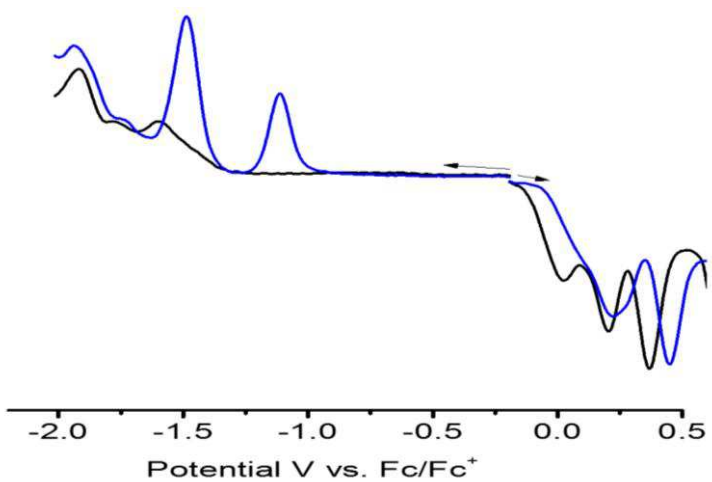

Fig. 4. Differential pulse voltammograms of $(TPA)_3$ZnP-ZnPc in the absence (black line) and presence (blue line) of stoichiometric amounts of C_{60}Im in DCB containing 0.1 M (n-$Bu_4N)ClO_4$. Scan rate = 5 mV/s, pulse width = 0.25 s, pulse height = 0.025 V.

diminished currents with an anodic shifts in the range of 20-75 mV suggesting participation of both ZnP and ZnPc entities in the conjugate formation, as shown in Scheme 1. On the cathodic side, additional peaks corresponding to C_{60}Im reduction, at the expected potentials,[23] were also observed.

Free-energy calculations for charge-recombination (ΔG_{CR}) and charge-separation (ΔG_{CS}) processes were performed according to the following equations based on Rehm-Weller approach,[28]

$$-\Delta G_{CR} = (E_{ox} - E_{red}) + \Delta G_S \quad (1)$$

$$-\Delta G_{CS} = \Delta E_{00} - (-\Delta G_{CR}) \quad (2)$$

where ΔG_{CR} and ΔG_{CS} refer to free-energy change for charge recombination and charge separation, respectively, and ΔE_{00} correspond to the singlet state energy of each zinc tetrapyrroles (2.04 eV for $^1(TPA)_3ZnP^*$, and 1.84 eV for $^1ZnPc^*$). The E_{ox} and E_{red} represent the oxidation potential of the electron donor (zinc tetrapyrrole) and the reduction potential of the electron acceptor (C_{60}Im), respectively. ΔG_S refers to the static energy, calculated by using the 'Dielectric continuum model' according to the following equation,

$$-\Delta G_S = -(e^2/(4\pi\varepsilon_0))[(1/(2R_+)+1/(2R_-)-(1/R_{CC})/\varepsilon_S - (1/(2R_+) + 1/(2R_-))/\varepsilon_R) \quad (3)$$

where R_+ and R_- are the radii of the radical cation and radical anion, respectively, and R_{CC} is the center-center distances between donor tetrapyrrole and C_{60}. The symbols ε_R and ε_S refer to solvent dielectric constants for electrochemistry and photophysical measurements, respectively. The free energy change (ΔG_{CS}) was found to be -0.60 eV for ^{1}ZnPc* originated, and -0.68 eV from ^{1}ZnP* originated electron transfer reactions in the conjugate.

Fig. 5 shows an energy level diagram depicting different photochemical events in the $(TPA)_3$ZnP:ImC_{60}-ZnPc:ImC_{60} conjugate. From steady-state fluorescence studies, sequential energy transfer from ^{1}TPA* to ZnP, and from ^{1}ZnP* to ZnPc within $(TPA)_3$ZnP-ZnPc was evident. In the case of $(TPA)_3$ZnP:ImC_{60}-ZnPc:ImC_{60} conjugate, direct excitation of one of the

TPA entities would generate $(TPA)_2{}^1TPA^*ZnP:ImC_{60}$-$ZnPc:ImC_{60}$ that would undergo energy transfer (ENT-1) to produce $(TPA)_3{}^1ZnP^*:ImC_{60}$-$ZnPc:ImC_{60}$ excited state species. This species can also be obtained by direct excitation of ZnP in the conjugate (at 400 nm excitation of the femtosecond laser sytem this would be the main event). The deactivation of $^1ZnP^*$ would have at least three paths, viz., intersystem crossing (ISC) to populate $^3ZnP^*$ (orange path in Fig. 5) charge separation (CS-1) to produce $[(TPA)_3ZnP]^{\bullet+}:ImC_{60}{}^{\bullet-}$-$ZnPc:ImC_{60}$ radical ion pair (blue path), and energy transfer (ENT-2) to produce $(TPA)_3ZnP:ImC_{60}$-$^1ZnPc^*:ImC_{60}$ (red path). The

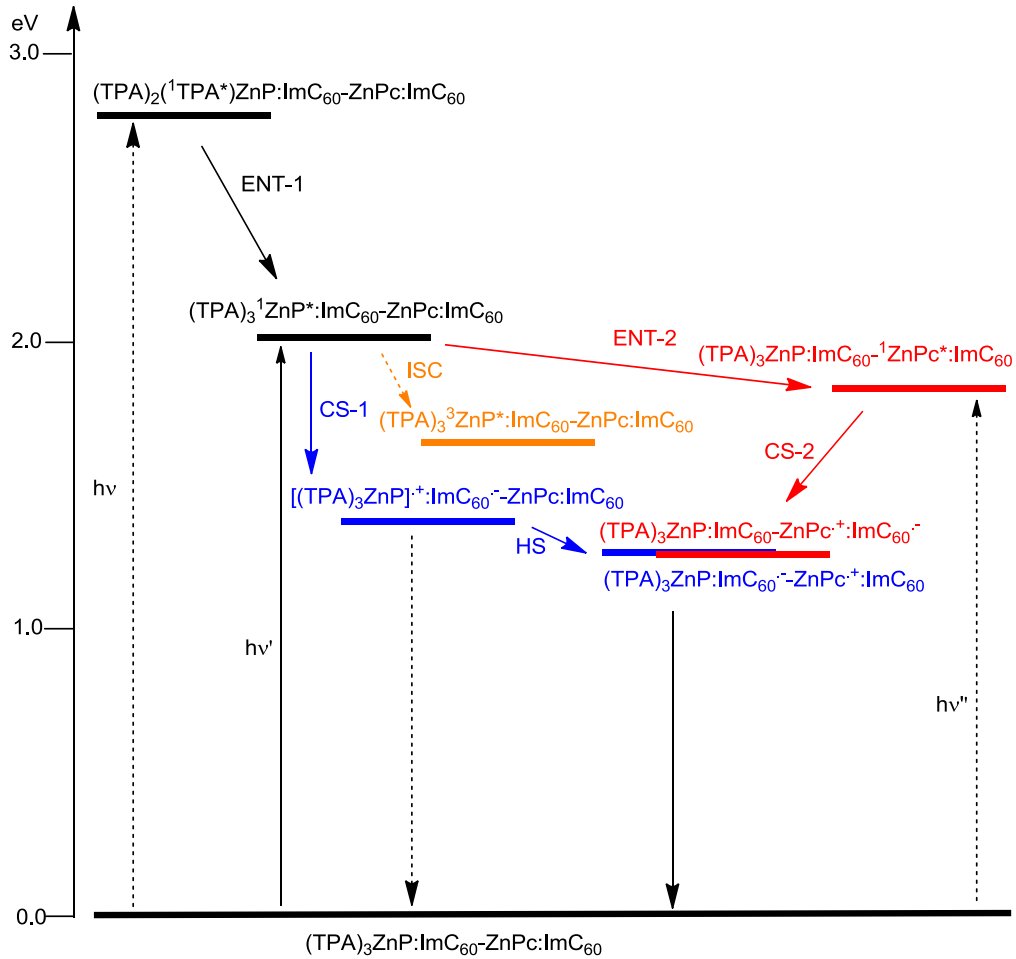

Fig. 5. Energy level diagram showing the different photochemical events of $(TPA)_3ZnP:ImC_{60}$-$ZnPc:ImC_{60}$ conjugate in dichlorobenzene. Energies of different states were evaluated from spectral and electrochemical studies. Solid arrow indicates major photo processes, dashed arrow indicates minor photo processes. A similar energy level diagram could be envisioned in toluene with the energy of the radical ion pairs about 150-200 mV above that in dichlorobenzene. Abbreviations: ISC = intersystem crossing, ENT = energy transfer, CS = charge separation and HS = hole shift.

newly formed ^{1}ZnPc* in the conjugate would undergo further electron transfer (CS-2) to produce $(TPA)_3ZnP:ImC_{60}$-$ZnPc^{\bullet+}:ImC_{60}^{\bullet-}$ radical ion pair. Subsequently, the $(TPA)_3ZnP^{\bullet+}:ImC_{60}^{\bullet-}$-$ZnPc:ImC_{60}$ radical ion pair would undergo a hole shift (HS) involving oxidatively facile ZnPc within the conjugate to produce $(TPA)_3ZnP:ImC_{60}^{\bullet-}$-$ZnPc^{\bullet+}:ImC_{60}$ radical ion pair. If hole shift process does occur, then the decay of $(TPA)_3ZnP^{\bullet+}$ would be faster than that would be observed in a radical ion-pair resulted in a structurally similar control complex, such as $(TPA)_4ZnP:ImC_{60}$. Importantly, the lowest energy radical ion-pairs, $(TPA)_3ZnP:ImC_{60}$-$ZnPc^{\bullet+}:ImC_{60}^{\bullet-}$ and $(TPA)_3ZnP:ImC_{60}^{\bullet-}$-$ZnPc^{\bullet+}:ImC_{60}$ are different in their traits in which the $C_{60}Im^{\bullet-}$ are located on different metallomacrocycle units. That is, on ZnPc in the former case and ZnP in the latter case. Since the radical anion and cation are spatially far in the case of $(TPA)_3ZnP:ImC_{60}^{\bullet-}$-$ZnPc^{\bullet+}:ImC_{60}$ (separated by ZnP), a relatively long-lived charge separated state could be anticipated in this case. In order to verify the occurrence of these events, transient absorption studies involving both femtosecond and nanosecond techniques have been performed, as summarized in the next section.

Femtosecond transient absorption studies

First, energy transfer in the $(TPA)_3ZnP$-ZnPc was investigated in a photochemically more stable solvent toluene. At the excitation wavelength of 400 nm, operating wavelength of femtosecond transient spectrometer, mainly the porphyrin unit is excited. Fig. 6a shows the spectral changes recorded during early time scale of $(TPA)_3ZnP$-ZnPc in toluene. Immediately after excitation, depleted peaks at 440, 550, 610 and 678 nm and positive peaks at 471, 576, 734, 770 nm were observed. The negative bands at 440, 550 and 610 nm corresponded to the ground state depletion of zinc porphyrin and 678 nm corresponded to the ground state depletion of zinc phthalocyanine with any contributions from stimulated emission. With time, the peak intensities of the 440 and 550 nm bands decreased with an increase of ZnPc stimulated band at 680 nm suggesting occurrence of energy transfer from the S_1 and S_2 states of ZnP. Fig. 6b shows the time profiles of the 440 and 680 nm peaks which suggests the energy transfer process to be completed by about 6 ps providing an energy transfer rate of $k_{ENT} \sim 1.6 \times 10^{11}$ s^{-1}. This rate of energy transfer is nearly an order of magnitude lower than that reported by us and others on porphyrin-phthalocyanine dyads in which the porphyrin ring lacked TPA entities.[17-19]

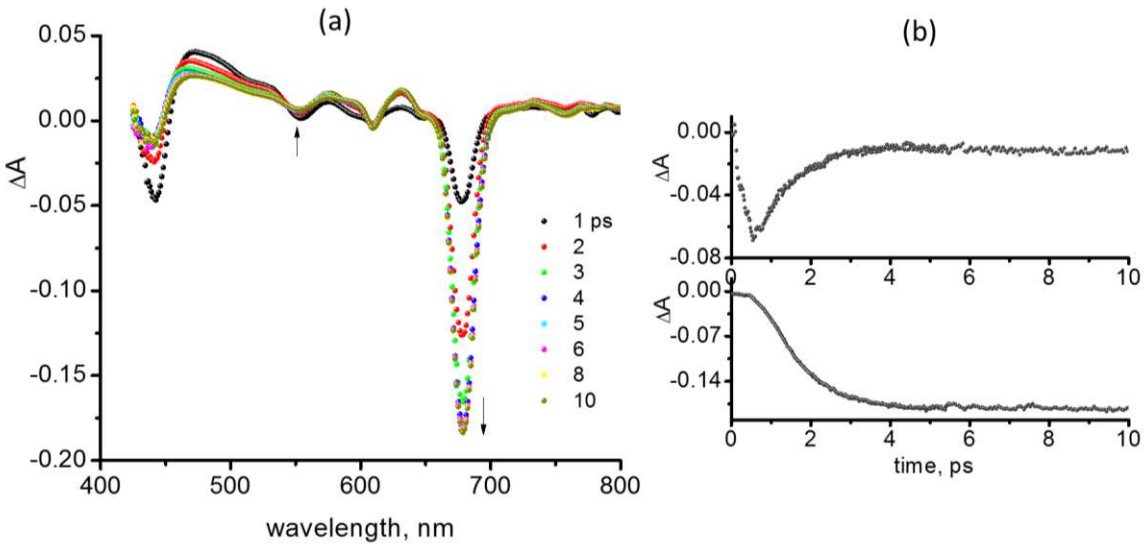

Fig. 6. Femtosecond transient spectra (100 fs pulse width at 400 nm) of $(TPA)_3ZnP$-ZnPc in Ar-saturated toluene at the indicated delay times revealing excited energy transfer. Fig. b shows time profile of the 440 nm 680 nm peaks.

To unravel the complex photochemical events occurring in $(TPA)_3ZnP$:ImC_{60}-ZnPc:ImC_{60} conjugate, shown in Fig. 5, few additional experiments were warranted. Towards this, first, photoinduced electron transfer in the $(TPA)_4ZnP$:ImC_{60} donor-acceptor system was needed to be established. Fig. 7a shows the femtosecond transient spectrum of $(TPA)_4ZnP$ at the indicated delay times. Immediately after excitation, depleted signals at 440, 550, and 600 nm, and positive peaks at 475 and 1420 nm were observed. The negative signals represent ground state depletion of $(TPA)_4ZnP$. The 1420 nm band has been assigned to singlet-singlet transition, similar to other zinc porphyrin derivatives reported in the literature.[29] The decay time constant for this signal was 1.74 ns (see Fig. 7c inset for time profile), close to the lifetime of $(TPA)_4ZnP$ determined from time-correlated single photon counting technique. The decay of singlet excited peaks was accompanied by new peaks at 480, 800 and 950(sh) nm bands corresponding to the triplet excited states of $(TPA)_4ZnP$ (see time profile of 480 nm peak in Figure inset).

Further, $(TPA)_4ZnP$ was chemically oxidized in DCB using nitronium hexafluoroantimonate, as shown in Fig. S4. The chemically generated $[(TPA)_4ZnP]^{\bullet+}$ revealed peaks at 770 and 1280 nm.[22] Appearance of these peaks in $(TPA)_4ZnP$:ImC_{60} conjugate upon photoexcitation would

imply charge separation in the conjugate with $[(TPA)_4ZnP]^{\bullet+}$ being one of the species of electron transfer process.

Fig. 7b shows the transient spectra of the $(TPA)_4ZnP:ImC_{60}$ conjugate formed in toluene. The decay of instanteneously formed $^1[(TPA)_4ZnP]^*$ was accompanied by transient peaks different from that of $^3[(TPA)_4ZnP]^*$. A new peak at 1020 nm corresponding to $C_{60}Im^{\bullet-}$ was clearly seen. However, the near-IR radical cation peak was overlapped with that of the singlet peak in this wavelength region. The spectrum of $(TPA)_4ZnP$ and $(TPA)_4ZnP:ImC_{60}$ recorded at 500 ps is shown in Fig. S5a which clearly shows features of $[(TPA)_4ZnP]^{\bullet+}$ at the expected wavelength regions. After reaching a maximum, the radical ion peaks started decaying indicating a charge recombination process. Fig. 7d inset shows the time profile of the $C_{60}Im^{\bullet-}$ peak at 1020 nm. It is clear from the decay profile that the radical ion pair persists beyond 3 ns,

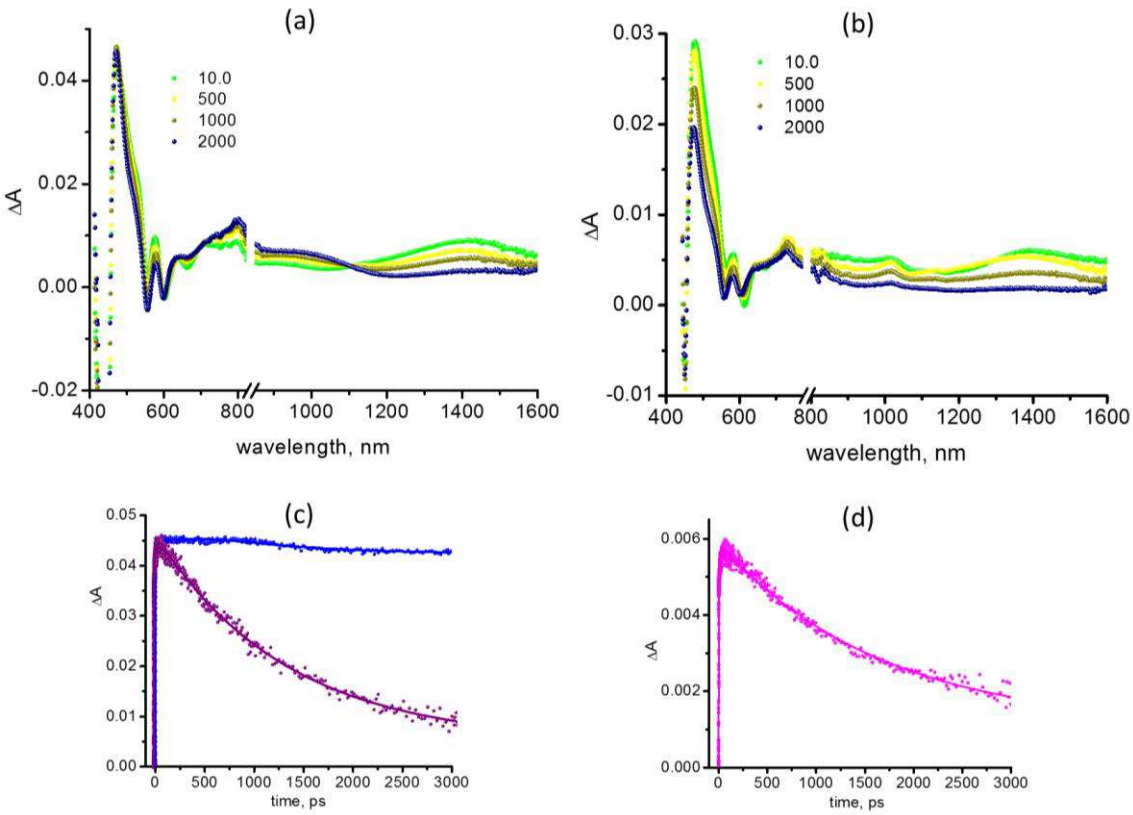

Fig. 7. Femtosecond transient spectra (100 fs pulse width at 400 nm) of (a) $(TPA)_4ZnP$ and (b) $(TPA)_4ZnP:ImC_{60}$ toluene at the indicated delay times. Fig. 7c shows the time profiles of 480 nm (blue) and 1420 nm (wine) peaks corresponding to the triplet and singlet peaks of $(TPA)_4ZnP$, respectively. Fig. 7d shows the time profile of the 1020 nm peak corresponding to $C_{60}Im^{\bullet-}$.

monitoring time window of our instrument. Under these conditions, the determined rate of charge recombination is only a lower limit. The determined rate of charge separation, k_{CS} and charge recombination, k_{CR}, were found to be 3.4 x 10^{10} s^{-1} and 5.3 x 10^{8} s^{-1}, respectively. These results revealed charge stabilization to some extent in the $(TPA)_4ZnP:ImC_{60}$ conjugate.

Fig. 8a shows transient visible-near IR spectra of $(TPA)_3ZnP$-ZnPc in toluene at indicated delay times covering the entire 3 ns monitoring time window. The spectral features were a combination of earlier discussed $(TPA)_4ZnP$ (Fig. 7a) and $(TPA)_3ZnP$-ZnPc (Fig. 6a). The instanteneously formed $^1[(TPA)_3ZnP]^*$-ZnPc revealed peaks corresponding to the ground state depletion (440 and 550 nm 610 nm) and singlet-singlet transition (1430 nm) corresponding to ZnP along with a band at 680 nm of ZnPc having contributions from ground state depletion and stimulated emission. At earlier time scales, the signal strength of 680 nm increased at the expense of ZnP peak intensities implying energy transfer. At later times, in the near-IR region, new weak peaks at 1360 and 1420 nm were also observed. The 1360 nm band appeared as a shoulder band to the main 1420 nm band. In order to interpret these peaks, femtosecond transient spectra of pristine ZnPc covering both visible and near-IR region was recorded. As shown in Fig. S6, pristine ZnPc also revealed these peaks implying that the near-IR bands in the spectra of $(TPA)_3ZnP$-ZnPc are due to $(TPA)_3ZnP$-$^1ZnPc^*$.

Next, $(TPA)_3ZnP:C_{60}Im$-ZnPc:ImC_{60} conjugates were formed to probe photoinduced electron transfer events. In the first set of experiment, $(TPA)_3ZnP$-ZnPc was complexed with only one equivalent of $C_{60}Im$ to check the accessability of both zinc centers to axial binding, as predicted from the nearly same binding constants and the competitive energy and electron transfer processes originating from $^1[(TPA)ZnP]^*$. Fig. 8b shows transient spectra of $(TPA)_3ZnP$-ZnPc under these conditions. Peaks corresponding to $C_{60}Im^{\bullet-}$ at 1020 nm, at 845 nm of $ZnPc^{\bullet+}$, and in the 1360 nm range corresponding to $[(TPA)_3ZnP]^{\bullet+}$ were observed. These results suggest the formation of $[(TPA)_3ZnP]^{\bullet+}$:$C_{60}Im^{\bullet-}$-ZnPc:ImC_{60} and $(TPA)_3ZnP:C_{60}Im$-$ZnPc^{\bullet+}$:$ImC_{60}^{\bullet-}$ radical ion pairs, although the complex formation process is incomplete due to insufficient amount of added $C_{60}Im$. The decay profiles of the $[(TPA)_3ZnP]^{\bullet+}$ at 1360 nm, $ZnPc^{\bullet+}$ at 845 nm and $C_{60}Im^{\bullet-}$ at 1020 nm are shown in Fig. 8b inset. It is interesting to note that the $[(TPA)_3ZnP]^{\bullet+}$ decays faster than that of $C_{60}Im^{\bullet-}$ and $ZnPc^{\bullet+}$ radical ions of the conjugate.

Next, the transient spectra of of $(TPA)_3ZnP$-ZnPc in the presence of 2.2 equivalents of $C_{60}Im$

to form $(TPA)_3ZnP:ImC_{60}$-$ZnPc:ImC_{60}$ conjugate was recorded as shown in Fig. 8c. Better developed radical ion-peaks of $[(TPA)_3ZnP]^{\bullet+}$, $C_{60}Im^{\bullet-}$ and $ZnPc^{\bullet+}$ were observed, suggesting involvement of both $(TPA)_3ZnP:ImC_{60}$ and $ZnPc:ImC_{60}$ donor-acceptor pairs of the $(TPA)_3ZnP:ImC_{60}$-$ZnPc:ImC_{60}$ conjugate in the charge separation process. Fig. S5b in ESI compares transient spectrum of $(TPA)_3ZnP:ImC_{60}$-$ZnPc:ImC_{60}$ conjugate with that of pristine $(TPA)_4ZnP$ at a delay time of 10 ps. Spectral signature peaks at 1360 nm corresponding to $[(TPA)_3ZnP]^{\bullet+}$ (overlaped with that of $^1[(TPA)_3ZnP]^*$ at 1420 nm) and $C_{60}Im^{\bullet-}$ at 1020 nm were observed. Importantly, at this time scale spectral features of $[(TPA)_3ZnP]^{\bullet+}$ were better developed than that of $ZnPc^{\bullet+}$ at 840 nm. These results are suggestive of the formation of $(TPA)_3ZnP^{\bullet+}:ImC_{60}^{\bullet-}$-$ZnPc:C_{60}Im$ radical ion pair as the major initial product. The time profiles (covering the entire 3 ns window) of the radical ions is shown in Fig. 8c inset while at shorter time scale (250 ps) is shown in Fig. 8d. From the time profiles in Fig. 8c inset, it is clear that the $[(TPA)_3ZnP]^{\bullet+}$ (wine colored plot) decays faster than that of $C_{60}Im^{\bullet-}$ (magenta) and $ZnPc^{\bullet+}$ (blue) radical ions of the conjugate. Moreover, the decay of $[(TPA)_3ZnP]^{\bullet+}$ is faster than the decay of earlier discussed $[(TPA)_4ZnP]^{\bullet+}:C_{60}Im^{\bullet-}$ (see Fig. 7b) while the decay of $ZnPc^{\bullet+}$ is much slower than that reported earlier $ZnPc^{\bullet+}:ImC_{60}^{\bullet-}$.[23c] These observations are suggestive of a hole shift from the cation radical of $(TPA)_3ZnP^{\bullet+}:ImC_{60}^{\bullet-}$-$ZnPc:ImC_{60}$ to ZnPc within the conjugate to yield $(TPA)_3ZnP:ImC_{60}^{\bullet-}$-$ZnPc^{\bullet+}:ImC_{60}$ radical ion-pair (process HS in Fig. 5) wherein the cation and anion radical species are separated by ZnP entity.

To secure additional evidence of this charge separation-hole shift process, the time profiles of the different radical ions were analyzed at early time scales as shown in Fig. 8d. By monitoring the growth of 1360 nm peak corresponding to $[(TPA)_3ZnP]^{\bullet+}$ (wine colored) a time constant of 37.2 ps was obtained that yielded a value for k_{CS} of 2.7 x 10^{10} s^{-1} for $[(TPA)_3ZnP]^{\bullet+}:ImC_{60}^{\bullet-}$-$ZnPc:ImC_{60}$ formation. This value compared with the earlier discussed k_{CS} of 3.4 x 10^{10} s^{-1} for $[(TPA)_4ZnP]^{\bullet+}:C_{60}Im^{\bullet-}$ formation. The k_{CS} obtained by monitoring the growth of $ImC_{60}^{\bullet-}$ in the $(TPA)_3ZnP:ImC_{60}$-$ZnPc:ImC_{60}$ conjugate was found to be 2.9 x 10^{10} s^{-1} (magenta), comparable to the rate of $[(TPA)_4ZnP]^{\bullet+}$ formation. Interestingly, the growth of $ZnPc^{\bullet+}$ monitored at 840 nm (blue line), stretched beyond 100 ps, and this growth was accompanied by initial decay of $[(TPA)_3ZnP]^{\bullet+}$ to some extent. The k_{CS} obtained for this process was found to be 9.2 x 10^9 s^{-1}. The difference between the k_{CS} values of $[(TPA)_4ZnP]^{\bullet+}$ and $ZnPc^{\bullet+}$ was ~10^9 s^{-1} that could be considered as rate of hole shift, k_{HS}, ignoring any contributions from $(TPA)_3ZnP:ImC_{60}$-

$ZnPc^{\bullet+}$:$ImC_{60}^{\bullet-}$, a product formed form direct excitation of ZnPc. The time profile of $[(TPA)_4ZnP]^{\bullet+}$:$C_{60}Im^{\bullet-}$ formation at 1360 nm is also shown in Fig. 8d (red line) for comparison with the time profile of $(TPA)_3ZnP^{\bullet+}$:$ImC_{60}^{\bullet-}$-ZnPc:ImC_{60} (wine). Faster decay of the latter due to the hole shift process compared to the former is evident from such comparision. Under the present conditions, the rise and decay of $C_{60}Im^{\bullet-}$ with multiple contributions makes it harder to

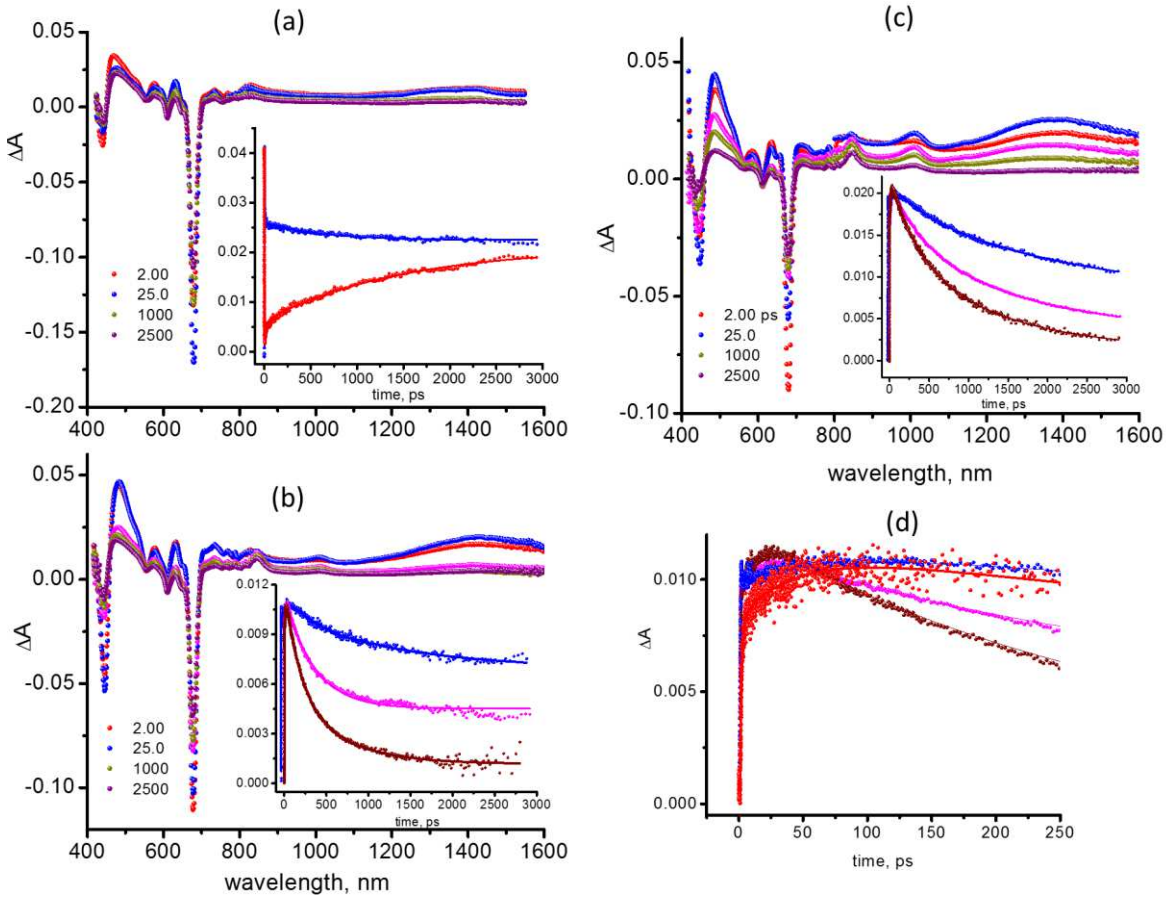

Fig. 8. Femtosecond transient spectrum of (a) $(TPA)_3ZnP$-ZnPc (inset: time profile of the 473 nm (blue) and 680 nm (red) peaks), (b) $(TPA)_3ZnP$-ZnPc in the presence of 1 eq. of $C_{60}Im$ (inset: time profiles of 842 nm (blue) 1020 nm (magenta), and 1360 nm (wine) peaks), and (c) $(TPA)_3ZnP$-ZnPc in the presence of 2.2 eq. of $C_{60}Im$ to form $(TPA)_3ZnP$:ImC_{60}-ZnPc:ImC_{60} conjugate (inset: time profiles of 842 nm (blue) 1020 nm (magenta), and 1360 nm (wine) peaks). Fig. 8d shows the time profile shown in Fig. 8c inset at shorter delay times representing rise and partial decay of the radical signals. The red line shows the time profile at shorter delay times of $(TPA)_4ZnP^{\bullet+}$:$ImC_{60}^{\bullet-}$ monitored at 1360 nm (the original data is shown in Fig. 7b). The spectra were recorded in toluene at the indicated time delays at the excitation wavelength of 400 nm.

analyze, however, persistence of both $ZnPc^{\bullet+}$ and $C_{60}Im^{\bullet-}$ beyond the 3 ns window is clear from the time profiles. The reported k_{CR} value for the radical ion pair, $ZnPc^{\bullet+}$:$ImC_{60}^{\bullet-}$ in the ZnPc:ImC_{60} conjugate from our recent study was 2.1 x 10^8 s^{-1} resulting in a lifetime of radical ion-pair of 4.8 ns.[23c] Persistence of the $ZnPc^{\bullet+}$ and $ImC_{60}^{\bullet-}$ radical ion signals in the $(TPA)_3$ZnP:ImC_{60}-ZnPc:ImC_{60} conjugate beyond 4.8 ns would ultimately mean the occurrence of charge separation/hole shift processes (CS-1/HS in Fig. 5) generating long-lived charge separated state.

Nanosecond transient absorption studies

In order to characterize the long-living $(TPA)_3$ZnP:$ImC_{60}^{\bullet-}$-$ZnPc^{\bullet+}$:ImC_{60} radical ion-pair, nanosecond transient studies were performed. Fig. S7a shows nanosecond transient spectrum of $(TPA)_4$ZnP at the indicated delay times in toluene. Peaks corresponding to ^{3}[$(TPA)_4$ZnP]* were present at 474, 810 and 970 nm. In fact the latter two peaks were broad enough to cover the spectral range of 650-1200 nm. From the decay of the 810 nm peak, a lifetime of 11.7 μs for $^3(TPA)_4$ZnP* was calcualted (see Fig. S7b for kinetic trace). As shown in Fig. S8, the conjugate $(TPA)_4$ZnP:ImC_{60} formed by complexing C_{60}Im revealed no detectable transient peaks supporting the formation of $[(TPA)_4ZnP]^{\bullet+}$:$ImC_{60}^{\bullet-}$, implicit lack of electron transfer from the $^{3[}(TPA)_4$ZnP]*.

The nanosecond spectrum of $(TPA)_3$ZnP:ImC_{60}-ZnPc:ImC_{60} conjugate, recorded at 32 and 68 ns delay times as shown in Fig. 9, revealed peaks at 840 and 1020 nm providing evidence for the existence of $ZnPc^{\bullet+}$ and $C_{60}Im^{\bullet-}$ species at these delay times. Since the $[(TPA)_3ZnP]^{\bullet+}$:$ImC_{60}^{\bullet-}$-ZnPc:ImC_{60} and $(TPA)_3$ZnP:ImC_{60}-$ZnPc^{\bullet+}$:$C_{60}Im^{\bullet-}$ radical ion pair are short lived (0.65 ns from decay profile of $[(TPA)_3ZnP]^{\bullet+}$ in Fig. 8c, and 4.8 ns for $ZnPc^{\bullet+}$), this could only be attributed to the presence of $(TPA)_3$ZnP:$ImC_{60}^{\bullet-}$-$ZnPc^{\bullet+}$:ImC_{60} radical ion pair, that is, the product of CS-1/HS in Fig. 5. At higher time scale, peaks corresponding to ^{3}[$(TPA)_3$ZnP]* started to develop (from unbound $(TPA)_3$ZnP in solution), however, the radical ion-pair signatures were obvious event in the spectrum collected at 104 ns. Notably, no $ZnP^{\bullet+}$ signal at 770 nm or 1360 nm was observed, suggesting lack of long-living $[(TPA)_3ZnP]^{\bullet+}$:$ImC_{60}^{\bullet-}$-ZnPc:ImC_{60} radical ion-pair at this time scale, as predicted from femtosecond transient studies. The ~100 ns lifetime of $(TPA)_3$ZnP:$ImC_{60}^{\bullet-}$-$ZnPc^{\bullet+}$:ImC_{60} radical ion pair is over 20 times greater than that reported for $ZnPc^{\bullet+}$:$ImC_{60}^{\bullet-}$ radical ion-pair ZnPc:ImC_{60}, being 4.8 ns. These

results support charge separation/hole migration via CS-1/HS route in Fig. 5 to produce long living $(TPA)_3ZnP:ImC_{60}^{\bullet-}$-$ZnPc^{\bullet+}:C_{60}Im$ radical ion-pair, with the radical cation and radical anion separated by a ZnP entity in the supramolecular conjugate.

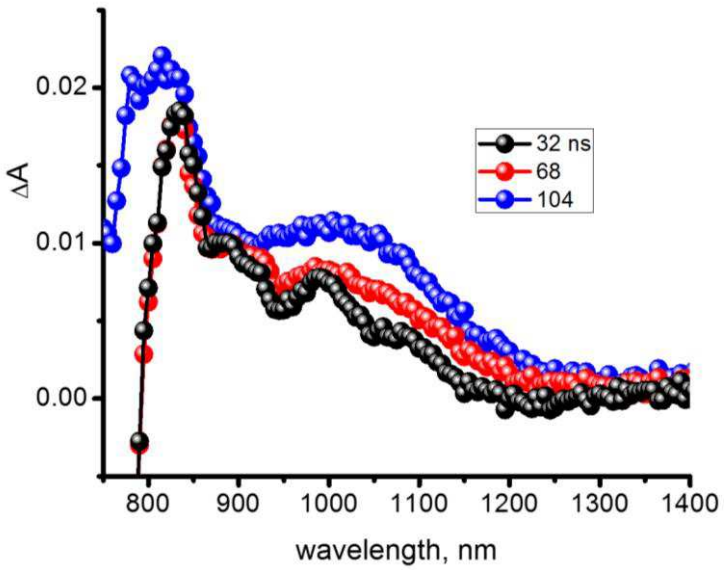

Fig. 9. Nanosecond transient spectra at the indicated delay times of $(TPA)_3ZnP:ImC_{60}$-$ZnPc:ImC_{60}$ conjugate in Ar-saturated toluene at the excitation wavelength of 430 nm.

It is worth pointing out here that in the previous studies involving zinc porphyrin-zinc phthalocyanine-fullerene derived supramolecular conjugates, it was not possible to establish such a CS/HS process leading to a long-lived radical ion-pair, wherein a relatively short-lived $ZnPc^{\bullet+}$-$C_{60}^{\bullet-}$ radical ion-pair with no detectable spectral signature supporting $ZnP^{\bullet+}$-$C_{60}^{\bullet-}$ radical ion-pair formation was observed.[17-19] Although both structural and electronic factors of the supramolecular assembly could contribute to this, the relatively slow energy transfer from excited zinc porphyrin to zinc phthalocyanine which would competitively promote electron transfer from singlet excited zinc porphyrin to the coordinated fullerene yielding $ZnP^{\bullet+}:C_{60}Im^{\bullet-}$ radical ion-pair could be considered to be the main contributing factor. As discussed earlier, the product of this charge separation-1 process, $ZnP^{\bullet+}:ImC_{60}^{\bullet-}$ would subsequently undergo a hole transfer process involving ZnPc to yield the long-lived $(TPA)_3ZnP:ImC_{60}^{\bullet-}$-$ZnPc^{\bullet+}:C_{60}Im$ radical ion pair within the conjugate. The present study delineates the importance of multi-modular supramolecular systems to derive new mechanistic and kinetic routes to accomplish the desired end product of artificial photosynthesis.

Summary

The newly synthesized and characterized photosynthetic antenna-reaction center model compound has been shown to undergo multi-step energy transfer processes, viz., ^{1}TPA* to ZnP and ^{1}ZnP* to ZnPc, funneling most of the near UV-visible radiation. The donor-acceptor conjugate formed upon assembling fullerene revealed charge separated states originating from both ^{1}ZnP* and ^{1}ZnPc* within the $(TPA)_3ZnP:ImC_{60}$-ZnPc:ImC_{60} conjugate. Interestingly, the charge separated state, $[(TPA)_3ZnP]^{\bullet+}:ImC_{60}^{\bullet-}$-ZnPc:$ImC_{60}$ originated from ^{1}ZnP* yielded $(TPA)_3ZnP:ImC_{60}^{\bullet-}$-$ZnPc^{\bullet+}:ImC_{60}$ radical ion-pair via a hole transfer mechanism in which the radical cation and radical anion were separated by the ZnP entity. Due to the distant location of the radical cation and radical anion (ZnP acting as a spacer), the charge recombination process was slowed down. The lifetime of the final charge separated state was about 100 ns which was over 20 times greater compared to the lifetime of $ZnPc^{\bullet+}:ImC_{60}^{\bullet-}$ radical ion-pair. The present multi-modular, donor-acceptor building strategy found to be an elegant approach to capture wide-band light and produce long-lived charge separated state.

Experimental Section

Chemicals. Buckminsterfullerene, C_{60} (+99.95%) was from SES Research, (Houston, TX). All the reagents were from Aldrich Chemicals (Milwaukee, WI) while the bulk solvents utilized in the syntheses were from Fischer Chemicals. Tetra-*n*-butylammonium perchlorate, $(n\text{-}Bu_4N)ClO_4$, used in electrochemical studies was from Fluka Chemicals. The synthesis of $C_{60}Im$ is given elsewhere.[23]

Syntheses of $(TPA)_3ZnP$-ZnPc. Scheme 2 outlines the methodology developed for the syntheses of target compounds. Details are given below.

4-(4-Formylphenoxy)phthalonitrile. 4-Nitrophthalonitrile (1 g, 5.77 mmol) and 4-hydroxybenzaldehyde (705 mg, 5.77 mmol) was stirred in DMF (30 ml) for 72 hours under nitrogen at room temperature. During this process, potassium carbonate (4 g, 29 mmol) was added to the mixture within the first 2 hours in four equal portions. After that the whole solution was poured into 100 ml ice water and filtered. After filtration, the residue was collected and washed first with cold methanol and then with cold hexanes, to get the desired compound as a

white powder. Yield- 1.2 gm (65%). ^{1}H NMR ($CDCl_3$; 400 MHz). δ, ppm = 6.90 (d, 2H, Ar-H), 7.42 (s, 1H, Ar-H), 7.74 (d, 2H, Ar-H), 7.90 (s, 1H, Ar-H), 8.20 (s,1H, Ar-H), 9.95 (s, 1H, -CHO).

Synthesis of [5-(4-(4-phenoxy)phthalonitrile)-10,15,20-tris(4-diphenylaminobenzene) porphyrin]. 4-(4-Formylphenoxy) phthalonitrile (500 mg, 2 mmol), 4-(diphenylamino)benzaldehyde (1.64 g, 6 mmol) and pyrrole (560 µl, 8 mmol) were kept in 500 ml RB flask and refluxed with propionic acid (120 ml) for 4 hours. After cooling the mixture to room temperature, the solvent was removed under reduced pressure and the crude product was purified over silica column. The desired compound was eluted by 100% chloroform. Yield - 10%. ^{1}H NMR ($CDCl_3$; 400 MHZ). δ, ppm = -2.85 (s, 2H, -NH), 7.05 (m, 12H, Ar-H), 7.35 (m, 24H, Ar-H), 7.58 (m, 2H, Ar-H), 7.92 (m, 2H, Ar-H), 8.03 (m, 6H, Ar-H), 8.18 (m, 1H, Ar-H), 8.25 (m, 1H, Ar-H), 8.32 (m, 1H, Ar-H), 8.80 (m, 2H, β-pyrrole H's), 8.88 (m, 6H, β-pyrrole H's).

Synthesis of $(TPA)_3$ZnP-ZnPc. A mixture of [5-(4-(4-phenoxy) phthalonitrile)-10,15,20-tris(4-diphenylaminobenzene) porphyrin] (120 mg, 0.095 mmol), 4-tert-butyl phthalonitrile (175 mg, 0.95 mmol) and $ZnCl_2$ (272 mg, 2 mmol) were kept in 100 ml RB flask under nitrogen for 20 minutes. Then, 2-dimethylaminoethanol (5 ml) was added and whole mixture was refluxed for 16 hours under nitrogen. After cooling the mixture to room temperature, the solvent was removed and the crude product was purified over silica column. The desired dyad was eluted by with $CHCl_3$:MeOH (95:5, v/v). % Yield = 12%. ^{1}H NMR ($CDCl_3$: 400 MHz). δ, ppm = 1.25-1.55 (m, 27H, tert-butyl H's), 7.10 (m, 12H, Ar-H), 7.45 (m, 24H, Ar-H), 7.58-7.68 (m, 4H, Ar-H), 8.18 (m, 6H, Ar-H), 8.85 (m, 2H, β-pyrrole H's), 8.95 (m, 6H, β-pyrrole H's), 9.2-9.4 (br, 12H, Pc-α-H's). MALDI-TOF, calculated = 1939.99, found – 1939.45.

Spectral Measurements. The UV-visible spectral measurements were carried out with a Shimadzu Model 2550 double monochromator UV-visible spectrophotometer. The fluorescence emission was monitored by using a Varian Eclipse spectrometer. A right angle detection method was used. The ^{1}H NMR studies were carried out on a Varian 400 MHz spectrometer. Tetramethylsilane (TMS) was used as an internal standard. Differential pulse voltammograms were recorded on an EG&G PARSTAT electrochemical analyzer using a three electrode system. A platinum button electrode was used as the working electrode. A platinum wire served as the

counter electrode and an Ag/AgCl electrode was used as the reference electrode. Ferrocene/ferrocenium redox couple was used as an internal standard. All the solutions were purged prior to electrochemical and spectral measurements using argon gas.

Femtosecond pump-probe transient spectroscopy. Femtosecond transient absorption spectroscopy experiments were performed using an Ultrafast Femtosecond Laser Source (Libra) by Coherent incorporating diode-pumped, mode locked Ti:Sapphire laser (Vitesse) and diode-pumped intra cavity doubled Nd:YLF laser (Evolution) to generate a compressed laser output of 1.45 W. For optical detection, a Helios transient absorption spectrometer coupled with femtosecond harmonics generator both provided by Ultrafast Systems LLC was used. The source for the pump and probe pulses were derived from the fundamental output of Libra (Compressed output 1.45 W, pulse width 100 fs) at a repetition rate of 1 kHz. 95% of the fundamental output of the laser was introduced into harmonic generator which produces second and third harmonics of 400 and 267 nm besides the fundamental 800 nm for excitation, while the rest of the output was used for generation of white light continuum. In the present study, the second harmonic 400 nm excitation pump was used in all the experiments. Kinetic traces at appropriate wavelengths were assembled from the time-resolved spectral data. Data analysis was performed using Surface Xplorer software supplied by Ultrafast Systems. All measurements were conducted in degassed solutions at 298 K.

Nanosecond laser flash photolysis. The studied compounds were excited by a Opolette HE 355 LD pumped by a high energy Nd:YAG laser with second and third harmonics OPO (tuning range 410-2200 nm, pulse repetition rate 20 Hz, pulse length 7 ns) with the powers of 1.0 to 3 mJ *per* pulse. The transient absorption measurements were performed using a Proteus UV-Vis-NIR flash photolysis spectrometer (Ultrafast Systems, Sarasota, FL) with a fibre optic delivered white probe light and either a fast rise Si photodiode detector covering the 200-1000 nm range or a InGaAs photodiode detector covering 900-1600 nm range. The output from the photodiodes and a photomultiplier tube was recorded with a digitizing Tektronix oscilloscope.

Acknowledgments

This work is financially supported by the National Science Foundation (Grant No. 1401188 to FD).

References

1. a) D. Gust, T. A. Moore in *The Porphyrin Handbook*, (Eds.: K. M. Kadish, K. M. Smith, R. Guilard), Academic Press: Burlington, MA. **2000**, Vol**.** 8, pp. 153-190; b) D. Gust, T. A. Moore and A. L. Moore, *Acc. Chem. Res*. 2001, **34,** 40-48, c) S. D. Straight, G. Kodis, Y. Terazono, M. Hambourger, T. A. Moore, A. L. Moore and D. Gust, *Nature Nanotechnol*. 2008, **3,** 280-283, d) D. Gust, T. A. Moore and A. L. Moore, *Acc. Chem. Res*. 2009, **42,** 1890-1898, e) D. Gust, T. A. Moore and A. L. Moore, *Faraday Discuss*., 2012, **155,** 9-26.
2. a) M.-J. Blanco, M. Consuelo Jimenez, J.-C. Chambron, V. Heitz, M. Linke and J.-P. Sauvage, *Chem. Soc. Rev*. 1999, **28,** 293-305, b) X. Dang, X, J. T. Hupp. *J. Photochem. Photobiol. A: Chemistry*, 2001, **143,** 251-256, c) V. Balzani, A, Credi and M. Venturi, *ChemSusChem*, 2008, **1,** 26-58, d) M. R. Wasielewski, *Acc. Chem. Res*. 2009, **42,** 1910-1921, (e) G. Renger, *Curr. Sci*. 2010, **98,** 1305-1319, f) D. G. Nocera, *Inorg. Chem*. 2009, **48,** 10001-10017.
3. a) D. M. Guldi, A. Rahman, V. Sgobba and C. Ehli, *Chem. Soc. Rev*. 2006, **35,** 471-487, b) J. N. Clifford, G. Accorsi, F. Cardinali, J. F. Nierengarten and N. Armaroli, *C. R. Chemie*., 2006, **9,** 1005-1013, c) N. Martin, L. Sanchez, M. A. Herranz, B. Illesca and D. M. Guldi, *Acc. Chem. Res*., 2007, **40,** 1015-1024, d) V. Balzani, A. Credi and M. Venturi, *ChemSusChem*, 2008, **1,** 26-58. e) G. Bottari, G. de la Torre, D. M. Guldi and T. Torres, *Chem. Rev*., 2010, **110,** 6768-6816, f) D. M. Guldi and V. Sgobba *Chem. Commun*., 2011, **47,** 606-610.
4. a) D. Holten, D. F. Bocian and J. S. Lindsey, *Acc. Chem. Res*., 2002, **35,** 57-69, b) J. S. Lindsey and D. F. Bocian, *Acc. Chem. Res*., 2011, **44,** 638-650.
5. a) H. Imahori and S. Fukuzumi, *Adv. Funct. Mater*., 2004, **14,** 525-536, b) S. Fukuzumi, *Pure Appl. Chem*., 2007, **79,** 981-991, c) S. Fukuzumi, *Phys. Chem. Chem. Phys.*, 2008, **10,** 2283-2297, d) S. Fukuzumi and T. Kojima, *J. Mater. Chem*., 2008, **18,** 1427-1439, e) S. Fukuzumi, T. Honda, K. Ohkubo and T. Kojima, *Dalton Trans*., 2009, 3880-3889, f) S. Fukuzumi and K. Ohkubo, *J. Mater. Chem*., 2012, **22,** 4575-4587.
6. a) M. E. El-Khouly, O. Ito, P. M. Smith and F. D'Souza, *J. Photochem. Photobiol. C*., 2004, **5,** 79-104, b) F. D'Souza and O. Ito, *Coord. Chem. Rev*., 2005, **249,** 1410-1422, c) R. Chitta and F. D'Souza, *J. Mater. Chem*., 2008, **18,** 1440-1471, d) F. D'Souza and O. Ito, *Chem. Commun*., 2009, 4913-4928, e) F. D'Souza, A. S. D. Sandanayak and O. Ito, *J.*

Phys. Chem. Letts. 2010, **1,** 2586-2593, f) F. D'Souza and O. Ito, *Chem. Soc. Rev*., 2012, **41,** 86-96, g) O. Ito and F. D'Souza, *Molecules*., 2012, **17,** 5816-5835, h) F. D'Souza and O. Ito, In *Multiporphyrin Array: Fundamentals and Applications*, (Ed. D. Kim), Pan Stanford Publishing: Singapore, 2012, Chapter 8, pp 389-437. i) S. Fukuzumi, K. Ohkubo, F. D'Souza and J. L. Sessler, *Chem. Commun.*, 2012, **48,** 9801-9815.

7. a) D. I. Schuster, K. Li and D. M. Guldi, *C. R. Chimie*, 2006, **9,** 892-908 b) R. Ziessel and A. Harriman, *Chem. Commun*., 2011, **47,** 611-631, c) A. C. Benniston and A. Harriman, *Coord. Chem. Rev*., 2008, **252,** 2528-2539, d) *Organic Nanomaterials* Eds. T. Torres and G. Bottari, Wiley-VCH, Weinheim, 2013, pp 187-204.
8. a) M. R. Wasielewski, *Chem. Rev*., 1992, **92,** 435-461, b) A. Osuka, N. Mataga and T. Okada, *Pure Appl. Chem*., 1997, **69,** 797-802, c) L. Flamigni, F. Barigelletti, N. Armaroli, J. P. Collin, I. M. Dixon, J. P. Sauvage and J. A. G. Williams, *Coord. Chem. Rev*., 1999, **190-192,** 671-682, d) F. Diederich and M. Gomez-Lopez, *Chem. Rev. Soc*., 1999, **28,** 263-277.
9. a) J. L. Sessler, C. M. Lawrence and J. Jayawickramarajah, *Chem. Soc. Rev*., 2007, **36,** 314-325. b) E. M. Pérez and N. Martín, *Chem. Soc. Rev*., 2008, **37,** 1512-1519, c) D. Gonzalez-Rodriguez, E. Carbonell and D. M. Guldi, *Angew. Chem. Int. Ed*., 2009, **48,** 8032-8036.
10. (*a*) A. Satake and Y. Kobuke, *Org. Biomol. Chem.*, 2007, **5**, 1679-1691. (*b*) J. L. Delgado, M. Á. Herranz and N. Martin, *J. Mater. Chem.*, 2008, **18**, 1417-1426.
11. a) *Photochemical Conversion and Storage of Solar Energy*, (Ed. J. S. Connolly), Academic Press: New York, 1981; b) *Molecular Level Artificial Photosynthetic Materials* (Ed. G. J. Meyer), Wiley, New York, 1997.
12. a) *Energy Harvesting Materials* (Ed.: D. L. Andrews), World Scientific, Singapore. **2005**; b) S. Gunes, H. Neugebauer and N. S. Sariciftci, *Chem. Rev.*, 2007, **107,** 1324-1338, c) N. Armaroli and V. Balzani, *Angew. Chem*. **2007**, *119*, 52; *Angew. Chem. Int. Ed.* 2007, **46,** 52-66. d) H. Imahori, T. Umeyama, S. Ito, *Acc. Chem. Res*., 2009, **42,** 1809-1818.
13. a) N. S. Lewis and D. G. Nocera, *Proc. Natl. Acad. Sci. U. S. A*., 2006, **103,** 15729-15735, b) P. V. Kamat, *J. Phys. Chem. C*, 2007, **111,** 2834-2860.
14. (*a*) T. Umeyama and H. Imahori, *Energy Environ. Sci.*, 2008, **1**, 120. (*b*) T. Hasobe, *Phys. Chem. Chem. Phys.*, 2010, **12**, 44-57.

15. a) G. Ulrich, R. Ziessel and A. Harriman, A. *Angew. Chem. Int. Ed*., 2008, **47,** 1184-1201. b) R. Ziessel, and A. Harriman, *Chem. Commun*., 2011, **47,** 611-631. c) M. El-Khouly, S. Fukuzumi and F. D'Souza, *ChemPhysChem*, 2014, **15,** 30-47.

16. a) F. D'Souza, P. M. Smith, M. E. Zandler, A. L. McCarty, M. Itou, Y. Araki and O. Ito, *J. Am. Chem. Soc.*, 2004, **126**, 7898-7907; b) E. Maligaspe, T. Kumpulainen, N. K. Subbaiyan, M. E. Zandler, H. Lemmetyinen, N. V. Tkachenko and F. D'Souza, *Phys. Chem. Chem. Phys*., 2010, **12**, 7434-7444, c) E. Maligaspe, N. V. Tkachenko, N. K. Subbaiyan, R. Chitta, M. E. Zandler, H. Lemmetyinen and F. D'Souza, *J. Phys. Chem. A*, 2009, **113**, 8478-8489, d) M. E. El-Khouly, C. A. Wijesinghe, M. E. El-Khouly, V. N. Nesterov, M. E. Zandler, S. Fukuzumi and F. D'Souza, *Chem. Eur. J.* 2012, **18,** 13844-13853, e) Y. Rio, W. Seitz, A. Gouloumis, P. Vázquez, J. L. Sessler, D. M. Guldi and T. Torres, *Chem. Eur. J.*, 2010, **16,** 1929-1940, f) F. D'Souza, C. A. Wijesinghe, M. E. El-Khouly, J. Hudson, M. Niemi, H. Lemmetyinen, N. V. Tkachenko, M. E. Zandler and S. Fukuzumi, *Phys. Chem. Chem. Phys.*, 2011, **13,** 18168-18178, g) Y. Liu, M. E. El-Khouly, S. Fukuzumi and D. K. P. Ng, *Chem. Eur. J.*, 2011, **17,** 1605-1613, h) F. D'Souza, A. N. Amin, M. E. El-Khouly, N. K. Subbaiyan, M. E. Zandler and S. Fukuzumi, *J. Am. Chem. Soc.*, 2012, **134,** 654-664, i) W.-J. Shi, M. E. El-Khouly, K. Ohkubo, S. Fukuzumi and D. K. P. Ng, *Chem. Eur. J.*, 2013, **19,** 11332-11341.

17. a) A. M. V. M. Pereira, A. R. M. Soares, A. Hausmann, M. G. M. S. Neves, A. C. Tome, A. M. S. Silva, J. A. S. Cavaleiro, D. M. Guldi and T. Torres, *Chem. Phys. Chem. Phys*., 2011, **13,** 11858-11863. b) R. F. Enes, J.-J. Cid, A. Hausmann, A. O. Trukhina, A. Gouloumis, P. Vazquez, J. A. S. Cavaleiro, A. C. Tome, D. M. Guldi and T. Torres, *Chem. Eur. J.* 2012, **18**, 1727-1736. c) M. V. M. Pereira, A. Hausmann, J. P. C. Tome, O. Trukhina, M. Urbani, M. G. P. M. S. Neves, J. A. S. Cavaleiro, D. M. Guldi and T. Torres, *Chem. Eur. J*., 2012, **18,** 3210-3219.

18. a) C. B. KC, K. Stranius, P. D'Souza, N. K. Subbaiyan, H. Lemmetyinen, N. V. Tkachenko and F. D'Souza, *J. Phys. Chem. C*, 2013, **117,** 763-773, b) C. B. KC, K. Ohkubo, P. A. Karr, S. Fukuzumi and F. D'Souza, *Chem. Commun*., 2013, **49,** 7614-7616. c) C. B. KC, G. N. Lim, F. D'Souza, *Chem. Eur. J*., 2014, **20**, 7725-7735.

19. a) E. Maligaspe, T. Kumpulainen, H. Lemmetyinen, N. V. Tkachenko, N. K. Subbaiyan, M. E. Zandler and F. D'Souza, *J. Phys. Chem. A*, 2010, **114,** 268-277. b) K. Stranius, R.

Jacobs, E. Maligaspe, H. Lemmetyinen, N. V. Tkachenko, M. E. Zandler and F. D'Souza, *J. Porphyrins Phthalocyanines*, 2010, **14,** 948-961, c) R. Jacobs, K. Stranius, E. Maligaspe, H. Lemmetyinen, N. V. Tkachenko, M. E. Zandler and F. D'Souza, *Inorg. Chem.*, 2012, **51,** 3656-3665.

20. a) H. Imahori, K. Tamaki, D. M. Guldi, C. Luo, M. Fujitsuka, O. Ito, Y. Sakata and S. Fukuzumi, *J. Am. Chem. Soc.*, 2001, **123,** 2607-2617, b) H. Imahori, D. M. Guldi, K. Tamaki, Y. Yoshida, C. P. Luo, Y. Sakata and S. Fukuzumi, *J. Am. Chem. Soc*., 2001, **123,** 6617-6628, c) H. Imahori, K. Tamaki, Y. Araki, Y. Sekiguchi, O. Ito, Y. Sakata and S. Fukuzumi, *J. Am. Chem. Soc*., 2002, **124,** 5165-5174, d) H. Imahori, Y. Sekiguchi, Y. Kashiwagi, T. Sato, Y. Araki, O. Ito, H. Yamada and S. Fukuzumi, *Chem.–Eur. J*., 2004, **10,** 3184-3196, e) D. M. Guldi, H. Imahori, K. Tamaki, Y. Kashiwagi, H. Yamada, Y. Sakata and S. Fukuzumi, *J. Phys. Chem. A*, 2004, **108,** 541-548.
21. a) H. Imahori, H. Norieda, H. Yamada, Y. Nishimura, I. Yamazaki, Y. Sakata and F. Fukuzumi, *J. Am. Chem. Soc*., 2001, **123,** 100-110, b) F. D'Souza, R. Chitta, S. Gadde, D. M. S. Islam, A. L. Shumacher, M. E. Zandler, Y. Araki and O. Ito, *J. Phys. Chem. B*, 2006, **110,** 25240-25250, c) A. Y. Smirnov, L. G. Mourokh, P. K. Ghosh and F. Nori, *J. Phys. Chem. C*, 2009, **113,** 21218-21224. d) S. H. Lee, A. G. Larsen, K. Ohkubo, Z. O. Cai, J. R. Reimers, S. Fukuzumi and M. J. Crossley, *Chem. Sci.*, 2012, **3,** 257-269.
22. a) F. D'Souza, S. Gadde, S. Islam, C. A. Wijesinghe, A. L. Schumacher, M. E. Zandler, Y. Araki and O. Ito, *J. Phys. Chem. A*, 2007, **111**, 8552-8560. b) C. A. Wijesinghe, M. E. El-Khouly, M. E. Zandler, S. Fukuzumi and F. D'Souza, *Chem. Eur. J.*, 2013, **19**, 9629-9638.
23. a) F. D'Souza, G. R. Deviprasad, M. E. Zandler, V. T. Hoang, A. Klykov, M. Perera, M. J. van Stipdonk, M. E. El-Khouly, M. Fujitsuka and O. Ito, *J. Phys. Chem. A*, 2002, **106,** 3243-3252. b) S. K. Das, B. Song, A. Mahler, V. N. Nesterov, A. K. Wilson, O. Ito and F. D'Souza, *J. Phys. Chem. C*, 2014, **118,** 3994-4006. c) S. K. Das, A. Mahler, A. K. Wilson and F. D'Souza, *ChemPhysChem*, 2014, **15,** 2462-2472.
24. a) J. R. Lakowicz, *Principles of Fluorescence Spectroscopy*, 3rd ed., Springer, Singaphore, 2006. b) M. E. El-Khouly, C. A. Wijesinghe, V. N. Nesterov, M. E. Zandler, S. Fukuzumi and F. D'Souza, *Chem. Eur. J*., 2012, **18**, 13844-13853.
25. H. A. Benesi and J. H. Hildebrand, *J. Am. Chem. Soc*., 1949, **71,** 2703-2707.

26. *Electrochemistry of Metalloporphyrins in Nonaqueous Media*, K. M. Kadish, E. V. Caemelbecke, G. Royal, In *The Porphyrin Handbook*; (Eds. K. M. Kadish, K. M., Smith, R. Guilard, R.), Academic Press: San Diego, CA, 2000, vol. 8, ch. 55.

27. a) Z. Zhao, T. Nyokong and M. D. Maree, *Dalton Trans.*, 2005, 3732-3737. b) N. K. Subbaiyan, I. Obraztsov, C. A. Wijesinghe, K. Tran, W. Kutner and F. D'Souza, *J. Phys. Chem. C*, 2009, **113,** 8982-8989.

28. a) D. Rehm and A. Weller, *Isr. J. Chem.*, 1970, **8,** 259-271, b) N. Mataga, H. Miyasaka, In *Electron Transfer*; (Eds. J. Jortner, M. Bixon), John Wiley & Sons: New York, 1999; Part 2, pp 431-496.

29. a) O. Schalk, H. Brands, T. S. Balaban, and A.-N. Unterreiner, *J. Phys. Chem. A* 2008, **112**, 1719-1729. b) D. B. Moravec, B. M. Lovaasen and M. D. Hopkins, *J. Photochem. Photobiol. A: Chemistry*, 2013, **254**, 20-24. c) M. Fathalla, J. C. Barnes, R. M. Young, K. J. Hartlief, S. M. Dyar, S. W. Eaton, A. A. Sarjeant, D. T. Co, M. R. Wasielewski, and J. F. Stoddart, *Chem. Eur. J.* 2014, **20**, 14690-14697. d) G. N. Lim, W. A. Webre, and F. D'Souza, *J. Porphyrins Phthalocyanines*, 2015, DOI: 10.1142/S108842461550008X.

Multi-modular, tris(triphenylamine) zinc porphyrin – zinc phthalocyanine –fullerene conjugate as a broad-band capturing, charge stabilizing, photosynthetic 'antenna-reaction center' mimic

C. B. KC, G. N. Lim, and F. D'Souza*

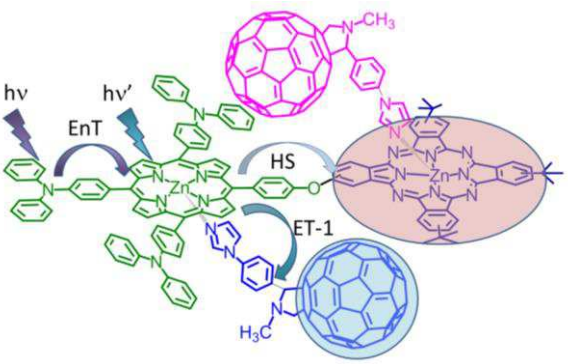

Charge stabilization as a result of electron transfer followed by hole-shift mechanism is demonstrated in a supramolecular multi-modular donor-acceptor assembly.